A Study of Diffusion- and Interface-Controlled Migration of the Austenite/Ferrite Front during Austenitization of a Case-Hardenable Alloy Steel

ERIC D. SCHMIDT, E. BUDDY DAMM, and SEETHARAMAN SRIDHAR

DOI: 10.1007/s11661-007-9208-4

Erratum to: METALLURGICAL AND MATERIALS TRANSACTIONS A, Vol. 38A, No. 2, February 2007, pp. 244–60
DOI: 10.1007/s11661-006-9029-x

THE color figures in this article were inadvertently printed in black and white in the printed issue. The article is reprinted in its entirety on the following pages.

ERIC D. SCHMIDT, Graduate Student, and SEETHARAMAN SRIDHAR, Professor, are with the Department of Materials Science and Engineering, Carnegie Mellon University, Pittsburgh, PA 15213, USA. Contact e-mail: sridhars@andrew.cmu.edu E. BUDDY DAMM, Principal Materials Engineer, is with The Timken Corporation, Canton, OH 44706-0930, USA.

The online version of the original article can be found under doi:10.1007/s11661-006-9029-x.
Article published online May 30, 2007.

A Study of Diffusion- and Interface-Controlled Migration of the Austenite/Ferrite Front during Austenitization of a Case-Hardenable Alloy Steel

ERIC D. SCHMIDT, E. BUDDY DAMM, and SEETHARAMAN SRIDHAR

Migrating austenite/ferrite interfaces in the ferrite regions of an alloy steel, containing 0.20 wt pct C, 0.87 wt pct Mn, and 0.57 wt pct Cr, with a ferrite/pearlite microstructure have been observed during austenitization by a high-temperature confocal scanning laser microscope in order to determine the mechanisms of transformation. The samples were subjected to isothermal (790 °C to 850 °C) and nonisothermal (0.5 °C to 20 °C/s) temperature profiles. The kinetic rates extracted from the observations were compared to models for long-range diffusion-controlled and interface reaction-controlled migration. The transition between the two mechanisms was found to occur at T_0, which defines the temperature and composition at which a partitionless phase transformation is possible. Occurrence of the partitionless, interface-controlled transformation was confirmed by an analysis of carbon distribution and microstructure before and after a sample was subjected to a particular thermal profile. The mobility of such interfaces was found to be in the range $1.6 \cdot 10^{-13}$ to $2 \cdot 10^{-12}$ $m^4 \cdot J^{-1} \cdot s^{-1}$, which is consistent with previous studies on interface-controlled migration of the reverse reaction, α to γ, during cooling of dilute substitutional iron alloys. The diffusion-controlled migration, at temperatures below T_0, was found to occur in two stages: an initial stage, at which the growth rate can be predicted by a semi-infinite diffusion model; and a second stage, at which the growth slows more rapidly, possibly due to the overlap of diffusion fields.

DOI: 10.1007/s11661-006-9029-x

I. INTRODUCTION

THE austenitization of medium to low-alloy carbon steels is an important part of many industrial heat treating procedures. It has not, however, received the more rigorous treatment that has been accorded to austenite decomposition into its several products (*e.g.*, References 1 through 6). This lack of detailed analysis can be explained through a number of prohibitive reasons, rooted in the nature of the ferrite-to-austenite transformation. The austenitization may proceed too rapidly in many cases for classical investigative methods, which may involve soaking a sample for various times and then evaluating a partially transformed microstructure through sectioning, polishing, and optical or electron microscopy. Even if this were not the case, the austenite simply cannot be retained for characterization in many circumstances, as it decomposes upon cooling. Due to the significant difficulty and expenditure of resources that might be dedicated to studying it, industrial practices mostly ignore the details of this process and simply use the fact that it does occur (*i.e.*, solution annealing) when designing heat treating procedures. As a result, one could argue that there has not been a strong driving force for research and analysis of the topic. It is, however, the opinion of the present authors that a fundamental understanding of the formation of austenite in alloy steels, in terms of kinetics, morphology, and mechanism, can significantly benefit thermal processing technology by improving the performance of the heat-treating and quenching process of alloy steels, reducing the number of steps and especially increasing the predictability of the final microstructure. Furthermore, the procedures used in the analysis contained here can certainly be applied in a study of other phase transformation phenomena.

There have been sporadic studies of austenite formation in iron and low-alloy steels during the last 40 years. These include experimental studies on the influence of starting microstructures on the transformation kinetics,[7–10] dilatometry,[9,11,12] and modeling of the transformation during continuous heating at varying scales of complexity.[13–16] As a result of these studies, there is some understanding of the austenite nucleation and growth process under limited conditions. For pure iron, austenite is assumed to nucleate at ferrite grain boundaries and the interface migration rate is controlled by the interface reaction (*i.e.*, the rate at which atoms jump across and are incorporated into the crystal on the opposite side of the interface).[7] When carbon is added to the iron, the growing austenite precipitates have a much higher concentration of carbon than the ferrite matrix, and thus carbon must be provided to the

ERIC D. SCHMIDT, Graduate Student, and SEETHARAMAN SRIDHAR, Professor, are with the Department of Materials Science and Engineering, Carnegie Mellon University, Pittsburgh, PA 15213, USA. Contact e-mail: sridhars@andrew.cmu.edu E. BUDDY DAMM, Principal Materials Engineer, is with The Timken Corporation, Canton, OH 44706-0930, USA.

Manuscript submitted August 4, 2006.

austenite/ferrite interface in order for it to remain at thermodynamic equilibrium as it proceeds into the ferrite. Long-range diffusion of carbon has been shown to be the rate controlling mechanism during austenitization of spheroidized ferrite-carbide aggregates.[10] In this case, isolated spherical carbide particles, several micrometers in diameter, act as the source of carbon as an austenite/ferrite interface proceeds outward from the carbide while the austenite/carbide interface proceeds inward until there is no carbide remaining. In a plain carbon eutectoid steel, there are extensive nucleation sites for austenite in lamellar eutectoid colonies due to the large number of ferrite/cementite boundaries in these regions. The rate of interface migration here is controlled by long-range diffusion of carbon along the interface (perpendicular to the lamellae) and will be determined by interlamellar spacing in the eutectoid colonies.[8] In steels exhibiting a microstructure containing both eutectoid colonies and ferrite grains, the eutectoid regions will initially transform during heating into regions of carbon-rich austenite, surrounded by untransformed carbon-poor ferrite grains. In order for the transformation to continue into the ferrite regions as the temperature increases, with the interface remaining at equilibrium, long-range diffusion of carbon (and, in some cases, other alloying elements) in the growing austenite toward (or away from) the interface must be considered.[9,13] For very slow austenite growth, *i.e.*, during intercritical annealing just above the eutectoid temperature, this mechanism has been confirmed by quenching the samples at different times and determining interface migration rates from the thickness of martensite (previously austenite) regions.[9] However, during continuous heating or at higher soaking temperatures, this method becomes unsuitable due to much faster transformation rates. For these conditions, other methods, such as dilatometry, must be used to experimentally measure transformation rates. Studies using this technique have relied upon assumptions about the starting microstructure (*i.e.*, ideal shape and uniform size of ferrite grains and eutectoid colonies) as well as the location and saturation of nucleation sites in order to compare proposed models of the transformation with the dilation data.[8,9,11,13–15] Previous studies by the present author[17,18] have confirmed some of the mechanisms proposed in the earlier work, specifically Roosz *et al.*[8] (austenite formation in lamellar eutectoid colonies) and Speich *et al.*[7] (austenite formation in pure iron) through the employment of *in-situ* confocal scanning laser microscopy (CSLM). However, one recently presented article[19] employing the same technique suggests near-linear growth behavior for austenite fronts, under certain isothermal conditions, within the ferrite grains of low-alloy carbon steels with mixed ferrite/eutectoid starting microstructures. These results appear to suggest that a long-range diffusion-controlled growth mechanism (*e.g.*, References 9 and 15) may not be accurate, at least for the temperatures investigated therein. A previous investigation by the current authors[20] used results from dilatometry to compare with the surface observations obtained in CSLM experiments, and suggested that the possibility of nonparabolic austenite front migration was consistent with the bulk transformation data.

The benefits of hot-stage CSLM microscopy have been discussed thoroughly in the literature (*e.g.*, References 17 and 21 through 23). With specific regard to the current investigation, the technique has been chosen because of the ability to resolve very slight topographical changes to a polished steel surface at elevated (up to 1600 °C) temperatures. The furnace that is employed in conjunction with the particular CSLM being used has the added capability of rapid heating, up to 40 °C/s. In order to ensure the accuracy of temperature measurements in the hot-stage CSLM system,[24] careful calibration of the temperature measurements, relative to the melting temperature of pure silver and copper metal, and the ferrite-to-austenite transition in pure iron, has been carried out. As a case study, 4118 carburizable steel with a starting microstructure consisting of ferrite and pearlite has been used in this investigation. Because the structure of this steel has well-defined ferrite grains and eutectoid regions with a normal lamellar structure (pearlite), a detailed analysis of the austenitization behavior with respect to the location of carbon in the structure can be obtained.

The objectives of this investigation are as follows: first, to further ensure the accuracy and usefulness of hot-stage confocal microscopy as a technique for analyzing solid-state phase transformations; second, to undergo a detailed investigation of the kinetics of austenite front migration during an important industrial process; and third, to use this kinetic analysis to discern the possible mechanisms of austenite front migration in the ferrite grains of mixed ferrite/eutectoid microstructure steels. This final objective will be considered in light of the possible interface-controlled and diffusion-controlled interface migration mechanisms (*e.g.*, References 25 through 27) and supported by the effect of carbon distribution on microstructural evolution during austenite decomposition after the austenitization.

II. MATERIALS AND EXPERIMENTAL METHODS

The 4118 steel that has been selected for this investigation is industrially produced, typically carburized, and used in power transmission applications such as gears or bearings. The composition and micrographs of the initial microstructure are provided in Table I and Figure 1, respectively. The initial (normalized) microstructure contains about a 70/30 mixture of ferrite and eutectoid colonies, and the eutectoid colonies exhibit a lamellar structure typical of pearlite, as shown in Figure 1(b). The samples were polished, using a Struers TegraSystem automatic polisher, by a sequence consisting of the following: a 220 grit resin-bonded diamond grinding disc, a 9-μm diamond suspension on a fine grinding disc, a 3-μm diamond suspension on a satin-woven acetate polishing cloth, a 1-μm diamond suspension on a synthetic short-nap velvet polishing cloth, and a 0.25-μm diamond suspension on another synthetic short-nap velvet cloth. Samples were thoroughly cleaned

Table I. Chemical Analysis Data for 4118 Steel Used in This Study (Weight Percent)

Sample	C	Mn	S	Ni	Cr	Mo	Si	Cu	Al
4118	0.20	0.87	0.030	0.10	0.57	0.09	0.30	0.23	0.042

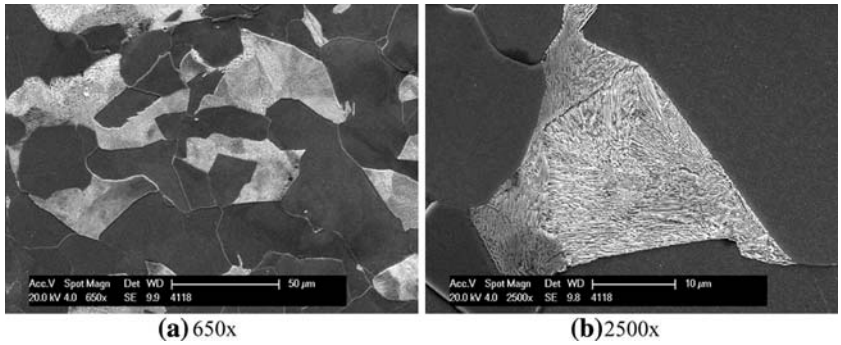

Fig. 1—Starting microstructure (etched with Nital) of the 4118 steel investigated in this study, showing (*a*) the overall mixed ferrite/eutectoid structure and (*b*) a eutectoid colony with lamellae oriented in a fairly uniform direction.

between polishing steps using precision, nonabrasive, residue-free detergent solution. A 1 pct nital solution was used to reveal ferrite/eutectoid structure as well as ferrite/ferrite grain boundaries. The samples were subjected, in the hot-stage CSLM, to a variety of thermal profiles in order to observe austenitization. A schematic of the hot-stage CSLM is shown in Figure 2. The details of its operation are widely available (*e.g.*, References 19, 21, and 23). For the current study, argon or helium gas was used (initial purity 10^{-5} atm O_2) as the atmosphere. The gas passed through an oxygen removal system composed of heated magnesium chips and copper turnings. An oxygen sensor has previously measured the p_{O2} of the argon gas obtained from this system to be no more than 10^{-14} atm. To begin an experiment, the furnace chamber is filled with argon, evacuated using a rotary vacuum pump (minimum chamber pressure of 1 in Hg/39 mbar/0.03 atm) for 10 minutes, refilled, evacuated, refilled, *etc.* for at least three cycles. After the final cycle, the argon is allowed to flow for at least 1 hour. The furnace chamber can be programmed to follow a specific thermal profile; this is specified in Table II. The chosen thermal cycles were similar to that practiced in industry for intercritical (*i.e.*, within a two-phase ferrite/austenite region) annealing, which may be used to produce a dual ferrite/martensite microstructure

Table II. Thermal Profile Data for CSLM Experiments

Heating Rate	Isothermal Hold	Quench
0.5 K/s	—	He gas
2.5 K/s	—	Ar gas
5 K/s	—	Ar gas
10 K/s	—	He gas
20 K/s	—	He gas
20 K/s	790 °C, 10 min	He gas
20 K/s	800 °C, 10 min	He gas
20 K/s	810 °C, 10 min	He gas
20 K/s	820 °C, 5 min	He gas
20 K/s	830 °C, 5 min	He gas
20 K/s	840 °C, 5 min	He gas
20 K/s	850 °C, 3 min	He gas
20 K/s	860 °C, 3 min	He gas
20 K/s	870 °C, 3 min	He gas

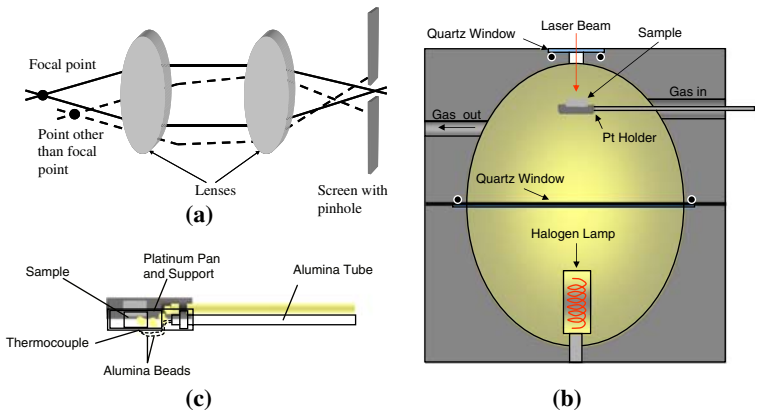

Fig. 2—Schematic of (*a*) confocal optics, where reflections from the surface can only be detected if the position of the surface is at the correct focal depth and thus "out of focus" features appear black rather than blurry; (*b*) elliptical furnace used as hot stage in CSLM, and (*c*) expanded view of sample holder used in the furnace chamber.

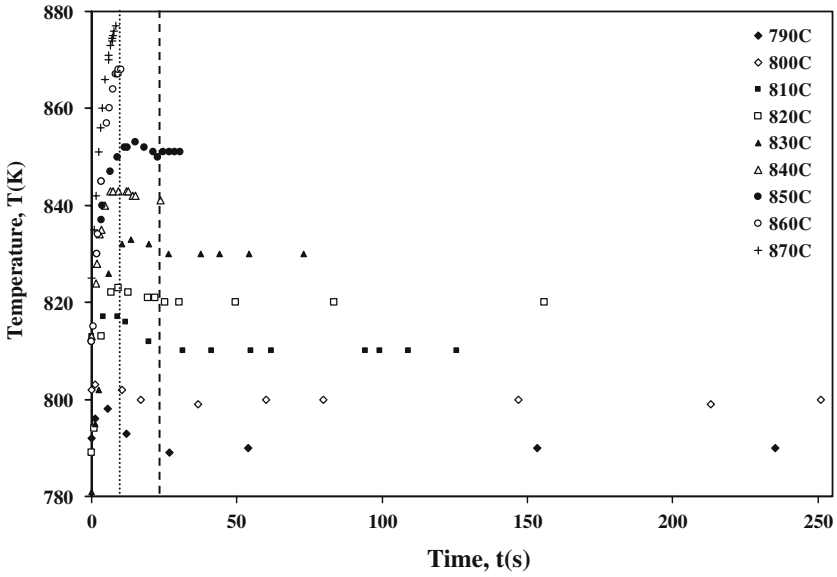

Fig. 3—Actual temperature vs time during isothermal CSLM experiments, based on measured points of austenite front migration in ferrite grains. Fine broken line indicates beginning of isothermal measurements for analysis, based on +/−5 K accuracy. Coarse broken line indicates the beginning of a strict (+/−1 K) isothermal temperature profile.

upon quenching,[9] or, heating to higher soaking temperatures, for complete austenitization prior to a variety of cooling steps. The ability of the microscope to reach and hold an isothermal temperature is indicated in Figure 3. The data points in this figure represent individual measurements of the migrating austenite/ferrite front; while the majority of the isothermal experiments reach a steady temperature for a significant portion of the transformation, it is apparent that at higher temperatures (> 850 °C), the temperature is not able to stabilize before the transformation is complete. The dashed line indicates the start of a strict regime, beyond which the temperature stays within one degree of the desired temperature; the majority of measurements below 840 °C fall beyond this line. However, in order to include the 840 °C and 850 °C experiments for analysis as isothermal experiments, all measurements obtained once the temperature stayed within about ± 5 °C, which represents points beyond the dotted line in the figure, have been used. At the highest temperatures, at which this is not possible, a polynomial equation representing the temperature profile is used for analysis where possible. During constant heating rate experiments, the measured temperatures follow a linear slope with time, with R^2 greater than 0.99 in all cases. The surface of the sample is recorded onto SVHS tape, at 30 frames per second, during the entire heat treating sequence. The video is digitized, using VIDEOWAVE* software, for subsequent analysis. Video is analyzed by toggling back and forth through a video and measuring the location of a front relative to where it first appeared on the screen. In order to ensure consistency, the furthest point on an austenite front from its starting location is used for each measurement. Great care has been taken to ensure accuracy of the data collected from the CSLM videos; each of the experiments has been analyzed repeatedly to ensure that the data are accurately represented. In order to ensure the accuracy of the temperature measurements, a set of calibration experiments were carried out using the known transformation temperature of pure materials. Small particles of silver and copper (a few milligrams each) were placed on the surface of a pure iron (99.995 pct) sample and heated slowly (~10 °C/min) to observe the melting of the silver and copper and the ferrite-to-austenite transformation of the iron. The austenite-to-ferrite transformation occurs before the particles have become liquefied, while the solid particles are not flat and only contact with the samples at particle edges; thus, it is not expected that any significant alloying occurs before the ferrite-to-austenite transformation. The relatively slow heating rate was used for the calibration tests in order to avoid any delay between the onset of melting in the silver and copper and the formation of a liquid metal pool; temperature measurements obtained during faster heating rates are consistent with those for the observed ferrite-to-austenite phase change for pure iron only. This calibration test was run several times and the temperature difference between the measured and expected thermodynamic temperatures was noted. The error in calibrated temperature measurement, determined by the range of measured temperatures compared to the average measured value for each calibration temperature, was determined to deviate by a maximum of ± 5 °C due to slight differences in the position of the sample relative to the thermocouple during each experiment. Micrographs of selected CSLM samples, before and after heat treating experiments, were obtained using a PHILIPS†

*VIDEOWAVE is a trademark of Sonic Solutions, Novato, CA

†PHILIPS is a trademark of Philips Electronic Instruments Corp., Mahwah, NJ

XL-30FEG scanning electron microscope. In select cases in which samples were quenched in helium immediately following austenitization, the resulting decomposition microstructure was etched and tinted, and a light optical method was used to produce micrographs.

III. RESULTS AND DISCUSSION

A. *CSLM Observations and Basis for Analysis*

In previous CSLM studies, interface migration has been observed for a range of transformations in steels (*e.g.*, References 17, 19, 21, and 24). In many of these cases, the surface structure is not preserved after the transformation, due to either rapid surface diffusion at high temperatures or subsequent transformations upon cooling. Therefore, the exact nature of the relief cannot be quantified and a general mechanism has not yet been proposed. Keeping this in mind, it appears quite reasonable to relate the surface relief fronts to the migration of interface boundaries.[22,23] An example of austenite front migration in a ferrite grain for the mixed ferrite/pearlite initial microstructure of 4118 steel, which is the subject of the current investigation, is shown in the series of images in Figures 4(a) through (d). A schematic that illustrates typical observations has been provided in Figure 5. The appearance of fronts in the CSLM can be explained by topographical changes caused by surface deformation due to the displacive[6,28,29] or dilatometric nature of a phase transformation. The appearance of a sharp contrast change at an interface may be adversely affected by surface diffusion, which can lead to smoothing of the surface,[30] especially for very slow growth rates. Other phenomena, such as the formation of nonmetallic phases (liquid or solid oxides, sulfides, *etc.*) on the surface, can also be observed. While in some cases (e.g., References 17 and 18) second-phase particles at or near the surface have been observed to act as nucleation sites, excessive surface oxidation will negatively affect the ability to elucidate the position of a front.

B. *Thermodynamic Considerations and the Massive Transformation*

In order to provide a framework within which kinetic data can be analyzed, it is necessary to know what phases may exist under a given set of conditions, the expected composition of these phases, and what kinds of interface dynamics are possible at the phase transformation boundary. As with most industrially obtained samples, the number of components in the 4118 steel prevents a simple, straightforward analysis, and suitable computer modeling software that can provide an accurate representation of thermodynamic data must be used. In addition, certain metastable equilibrium states have also been considered. Specifically, the temperature limit above which a partitionless transformation may occur in a two-phase equilibrium[26] is defined as T_0, the temperature at which two phases, at identical compositions, have the exact same free energy and can exist at metastable equilibrium at an interface. In multicomponent systems where an interstitial solute (*e.g.*, carbon in iron) has a diffusion coefficient several orders of magnitude larger than the substitutional solute elements, a situation of paraequilibrium may exist where only the interstitial element may vary in composition across the interface; the composition of the remaining elements remains constant in both phases. This is a useful condition for steel systems where long-range

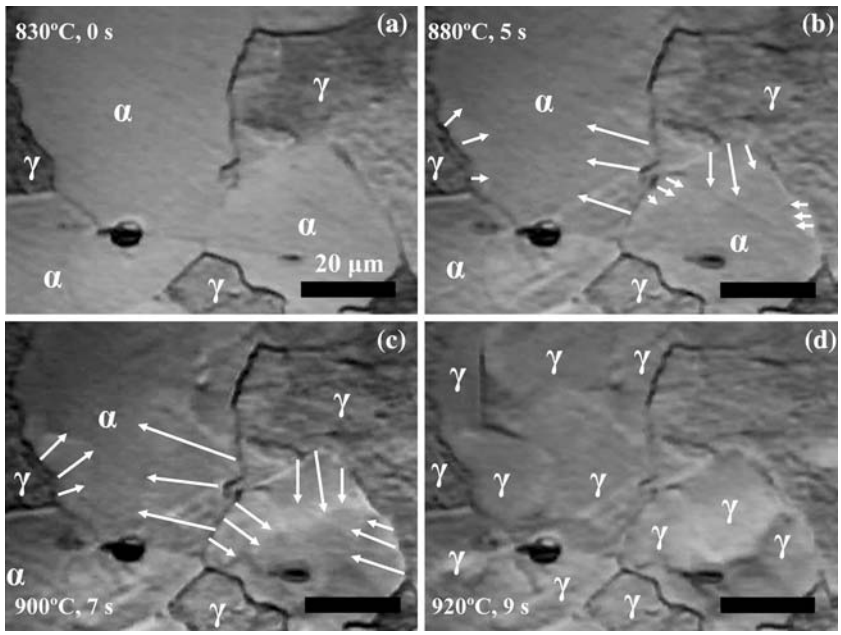

Fig. 4—(*a-d*): CSLM still image sequence of austenite formation in 4118 ferrite grains. Surrounding eutectoid regions have already transformed to austenite. Arrows indicate regions of austenite with moving interface boundaries relative to labelled ferrite regions. This sample was heated at 10 K/s during the transformation.

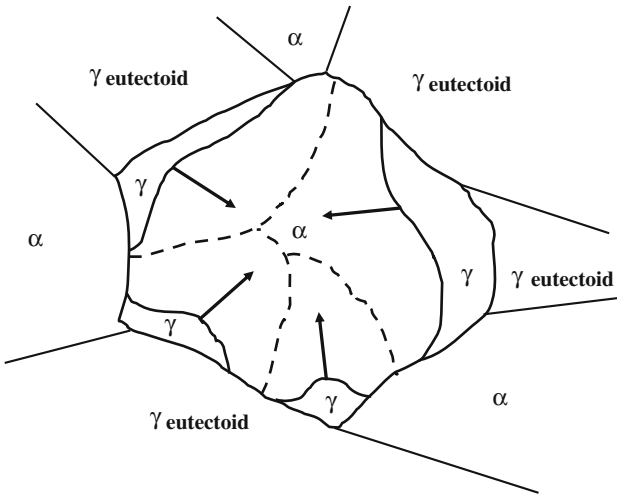

Fig. 5—A cartoon illustrating the general case of austenite fronts progressing in a ferrite grain.

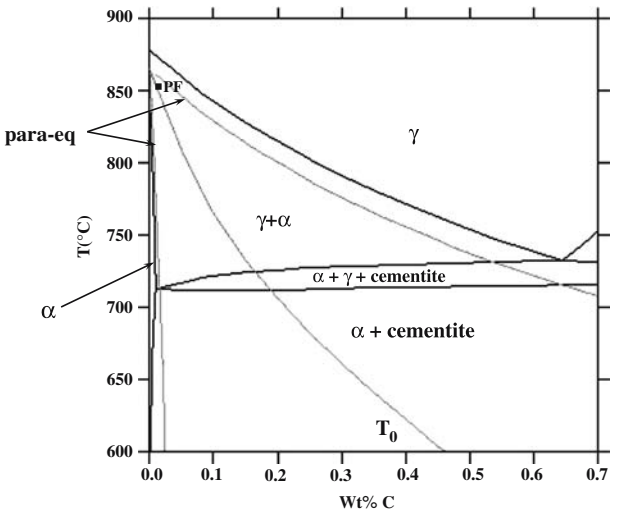

Fig. 6—Carbon isopleth for 4118 alloy. Black lines indicate equilibrium, grey lines indicate the para-equilibrium and T_0 (indicated). The point labeled 'PF' indicates an approximate temperature (855 °C) above which a partitionless transformation is possible in pro-eutectoid ferrite grains.

diffusion of carbon is often the rate controlling step during interface migration. THERMO-CALC[‡] has been used to construct a carbon isopleth diagram, shown in Figure 6, for the chemistry of interest; T_0 and paraequilibrium lines have been included and are labeled accordingly.

[‡]Thermo-Calc is a trademark of Thermo-Calc Software, Stockholm, Sweden

In order to use this diagram for analysis of on-heating experiments, we must make a few assumptions about the conditions during the decomposition of austenite when our samples were created. At temperatures below 800 °C, where the proeutectoid ferrite is precipitated, the diffusion coefficients of the alloying elements such as chromium and manganese are known to be at least four to six orders of magnitude lower than that of carbon (10^{-6} to 10^{-8} for carbon and 10^{-12} to 10^{-14} for Cr and Mn).[31,32,44,45] Based on an approximate ($t = x^2 \cdot D^{-1}$) estimate of diffusion time for the substitutional elements, at the distance scale in these samples (ferrite grain size of 10 to 40 μm), it would require days to years for decomposition to complete under full equilibrium conditions, *vs* seconds to minutes for paraequilibrium conditions. It is thus expected that paraequilibrium conditions existed at this time. Thus, the composition of substitutional alloying elements in the proeutectoid ferrite grains will be nearly identical to the bulk composition, and we can assume the same paraequilibrium lines will apply during austenitization of the ferrite. This also supports the validity of the T_0 line relative to proeutectoid ferrite, as it is determined by varying only the carbon composition to determine the T_0 temperature. This is supported by the fact that T_0 and paraequilibrium lines approach the same temperature at nil concentration of carbon. We will assume that any intergranular carbide precipitates that may have formed in the proeutectoid ferrite regions upon additional cooling (these can be seen as tiny specks of white in the ferrite regions of Figure 1(b)) have dissolved during heating, before austenitization, and that due to the small size and even distribution of these carbides, the resulting carbon gradients in the ferrite are rapidly homogenized. It is difficult to know the exact composition of carbon at which the eutectoid transformation would commence during a paraequilibrium decomposition of austenite, but the carbon concentration of proeutectoid ferrite should be given by the paraequilibrium line near the eutectoid temperature. The T_0 temperature at this composition has been labeled "PF" (proeutectoid ferrite) in Figure 6.

Two kinds of partitionless phase transformations have been widely recognized, termed massive and martensitic.[27] The conservative motion of interfaces under these conditions has been detailed extensively by Sutton and Balluffi.[33] The driving force for the movement of such an interface is simply the bulk free energy difference of the parent and precipitate phases at a given composition. If the interface proceeds by the uncorrelated (civilian) motion of atoms across the interface, the boundary will be only partly coherent, or altogether incoherent, and because these interfaces have few or no bonds across them that must be broken in order for the interface to migrate, transformation by this mechanism can occur very close to T_0. Such boundaries are generally planar in nature, although some curvature or faceting is usually observed and can proceed at a uniform velocity in any direction. These types of interfaces have been associated with massive transformations.[34,35] The overall starting microstructure of 4118 steel, prior to austenitization, is not uniform as is usually specified in a definition of the massive transformation.[26] However, if long-range diffusion is not a rate controlling step for migration of an interface in a particular ferrite grain in the present material, it seems reasonable to consider that grain, isolated from the rest

of the microstructure, to have the uniform, homogenous microstructure required by such a definition. In other words, an austenite front proceeding by a partitionless mechanism in a ferrite grain would be identical to an interface proceeding without diffusion in steel with a 100 pct ferrite starting microstructure. If a particular interface within a ferrite grain is migrating by the same mechanism, and meets all of the other requirements associated with a massive transformation, it follows that this term may also be used in the current investigation. This would occur above the temperature indicated by PF in Figure 6, and thus this temperature should represent a critical point with regard to the kinetic behavior of a migrating interface.

C. *CSLM: Nonisothermal Front Migration*

A set of CSLM images, for the 2.5 deg/s heating rate, is provided in Figures 7(a) through (e). An interesting observation from this set of images is that an austenite front actually appears to nucleate and then grow from an already existing austenite/ferrite interface within a ferrite grain. This front proceeds much more rapidly than the front from which it nucleated. This is a unique event within the set of experiments performed in this study, but makes an interesting statement about the non-necessity of austenite fronts to nucleate at carbon-rich (prior eutectoid) austenite grains. The front position has been plotted with respect to temperature for five heating rates in Figure 8. The temperature is proportional to time and the slope of the curves is therefore a rate. The curves are displayed in the context of the important thermodynamic condition T_0, such that one may see where a partitionless transformation is possible. At the slowest heating rate, 0.5 K/s, the observable transformation appears complete before T_0 is reached. This is consistent with the fact that, as indicated in Figure 6 by point A, a 100 pct austenite microstructure is possible (only *via* long-range diffusion of carbon) at any temperature above 800 °C for the bulk alloy composition of 0.2 wt pct carbon. For the remaining heating rates, however, the curves display a significant change as the temperature increases past T_0, with a relatively constant slope before and an increase in slope with temperature beyond. At temperatures below T_0, an approximately linear slope (constant velocity) is observed. In this temperature region, it is expected that parabolic decay of the long-range diffusion-controlled growth rate[27] and a constant increase in temperature, and therefore diffusion coefficients, are working divergently—resulting in the apparently constant velocity that is observed. Above T_0, when diffusion is no longer required for the front to migrate, the growth rate increases drastically and thus an interface reaction-controlled growth mechanism is expected to exist. This mechanism has been described, for pure iron, by the relationship[7]

$$v = \left(\frac{\delta \nu}{kT}\right) \exp\left(\frac{\Delta S^*}{k}\right) \exp\left(\frac{-\Delta H^*}{kT}\right) \Delta g^{\alpha \rightarrow \gamma} \qquad [1]$$

where v is the velocity of the interface; δ is the boundary width, assumed be 5 Å;[7] ν is the jump frequency; ΔS^* and ΔH^* are the activation entropy and enthalpy for migration of an atom across the interface, respectively; and $\Delta g^{\alpha \rightarrow \gamma}$ is the driving force for the reaction (per atom). The activation enthalpy for atoms across the boundary was approximated by the activation enthalpy for grain boundary diffusion in pure iron, as suggested by Shewmon;[36] Speich and Szirmae[7] used a value of 2.76×10^{-19} J/atom (166 kJ/mole). This value is consistent with that suggested by Brown and Ashby[37] for grain boundary diffusion in γ-iron. Because the jump frequency and activation

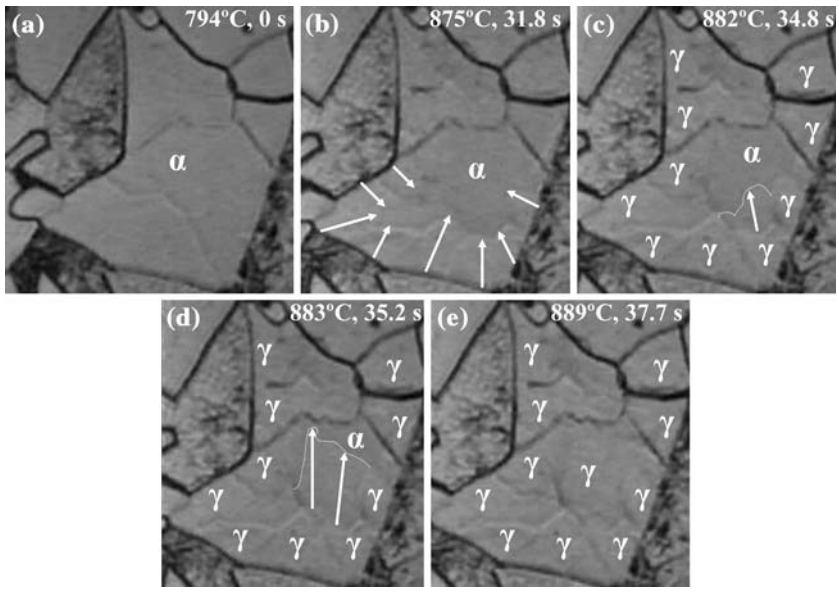

Fig. 7—(*a-e*): CSLM still images showing an austenite front (white dotted line) which originates from a migrating ferrite/austenite grain boundary during austenitization of a ferrite grain.

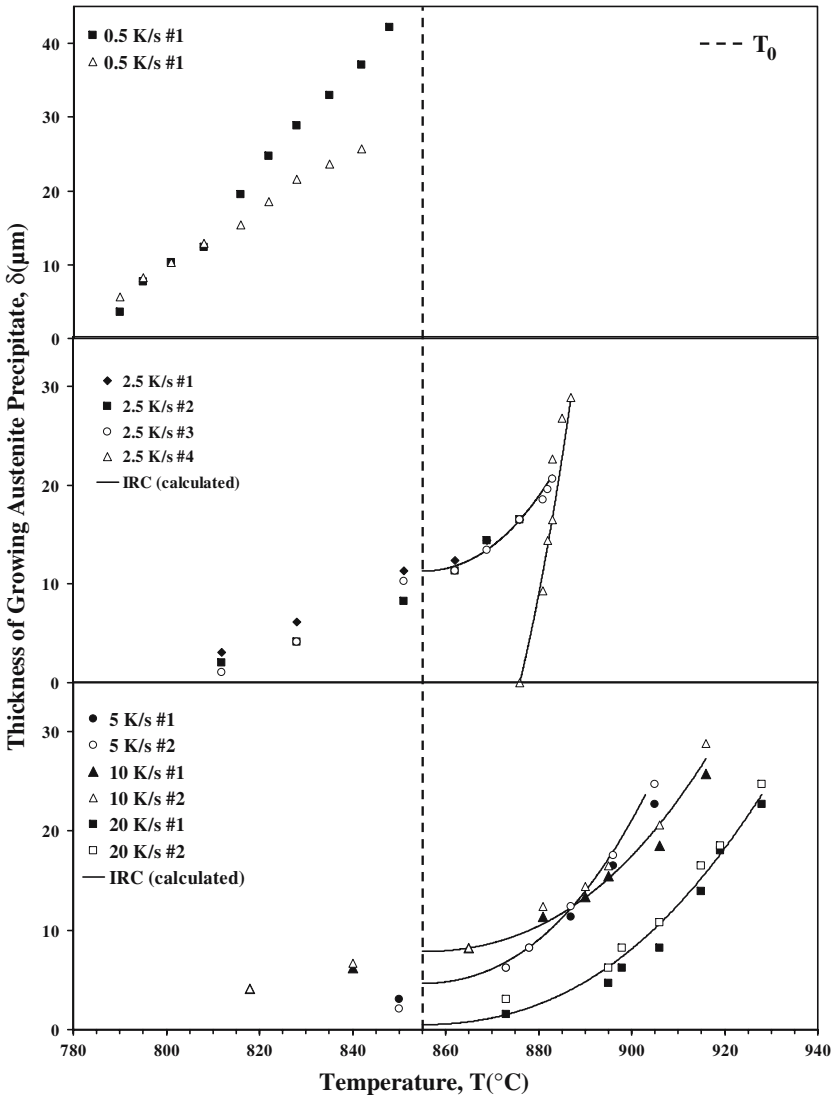

Fig. 8—Front migration data from CSLM for the constant heating rate experiments; important thermodynamic temperatures (with respect to ferrite grain composition) are included for comparison. Curves represent an interface reaction control model fit to the data.

entropy are not well known, the term $v \cdot \exp(\Delta S^*/k)$ was determined experimentally from data for pure iron; a maximum interface velocity of 1.6 cm/s was reported for 950 °C, where the driving force is 4.18×10^{-23} J/atom, and so this term is approximated to be 1.65×10^{17} s^{-1}.[7] The driving force for the transformation in the 4118 steel was assumed to be equal to that for pure iron, with the temperature of transformation equivalent to T_0. Thermodynamic calculation of free energy for Fe-Mn alloys at Mn concentrations varying between 0.05 and 0.50 wt pct and carbon less than 0.01 wt pct confirm that Mn additions may decrease the temperature of transformation but that the free energies relative to that temperature are nearly identical.[11] Therefore, this should be a reasonable approximation for fitting the experimental data, especially as the exponential term is influenced much more strongly by temperature than the driving force term.

In order to compare with position *vs* temperature curves produced by the CSLM data, this relationship has been integrated numerically, with respect to time, using the midpoint rule, with each time-step equal to 0.002 of the total time. Because time is directly proportional to temperature ($T = Kt$, where K is a constant equal to the heating rate), this result can be used to produce the desired relationship between position and temperature. The integration was done backward from the end of the transformation back to T_0. This was done because the early stages of interface-controlled growth may actually overlap with the long-range diffusion-controlled growth regime, as the driving force is relatively small just above T_0 and long-range diffusion may still dominate the growth rate. The resulting curves (denoted "IRC" for interface reaction control) are plotted in Figure 8 and show that Eq. [1] describes the interface migration quite well. The fronts that appeared to nucleate at existing austenite/ferrite interfaces are

represented by this model as well, although at a somewhat higher mobility. The increased mobility could indicate that there may have been an impurity drag environment building up at the prior migrating interface, which does not initially affect the new interface. Although the analysis supports the inference of a newly nucleated front, it cannot be absolutely ruled out that the appearance of the nucleating front results instead from an existing front that was growing from below the surface. For the highest temperature isothermal attempts (both above T_0) in which austenitization also proceeds under nonisothermal conditions, results were analyzed for consistency with the interface reaction control model. In this case, because the temperature profile was not linear, a polynomial fit of temperature *vs* time for the measured points at temperatures above T_0 was used in the integration. Figure 9 shows position *vs* time plots for these experiments and also shows excellent agreement between experimental data and the model. Once again, the curves denoted IRC represent the interface control model in Eq. [1]. The curves in all nonisothermal cases were fit to the data by varying the activation enthalpy until a good match was achieved. The value of this experimentally determined activation enthalpy varies between 232.6 and 248.8 kJ/mole, as indicated in Table III. These enthalpies are well within the range of recent measurements of activation energy for migration of high-angle grain boundaries in α-iron (200 to 400 KJ/mole), where the values vary significantly with the character of the boundary.[38] Even if most of the boundaries in the present investigation were very similar in character, it does not seem unreasonable to expect some slight variation in this value from front to front. Just above T_0, the calculated curves underestimate the growth rate (the rate is indicated by the slope), which suggests that carbon diffusion control exists until the driving force for the massive transformation (related to $T - T_0$) is sufficiently large. The temperature at which this seems to occur correlates well with the upper limit of paraequilibrium; this also suggests that some component of diffusion-controlled interface migration is still affecting the velocity of the interface in the range of paraequilibrium above T_0. Nonetheless, the rest of the data is well represented by the interface control model for these experiments. It is also expected that the long-range carbon diffusion-controlled front migration would only occur within the two-phase paraequilibrium region, as the low-temperature phase would become unstable (at any carbon concentration) above this temperature region, and the results for all constant heating rate experiments are consistent with this expected behavior. It should be noted, however, that the extracted values for activation enthalpies are to a good degree dependant on the choice of values that constitute the pre-exponential factor in Eq. [1],[18] and there is significant uncertainty regarding the magnitude of the pre-exponential factor.[39] Until more careful evaluation of this value can be undertaken, it seems prudent to consider the overall mobility of interface reaction-controlled moving

Table III. Experimentally Determined Activation Enthalpy for Several Experiments in Interface Reaction Control Regime (Temperature above T_0)

Experiment	Activation Enthalpy, ΔH^* (kJ/mole)
0.5 K/s	—
2.5 K/s (numbers 1–3)	248.8
2.5 K/s (number 4)	235.8
5 K/s	247.3
10 K/s	245.7
20 K/s	241.0
860°C	232.6
870°C	241.2

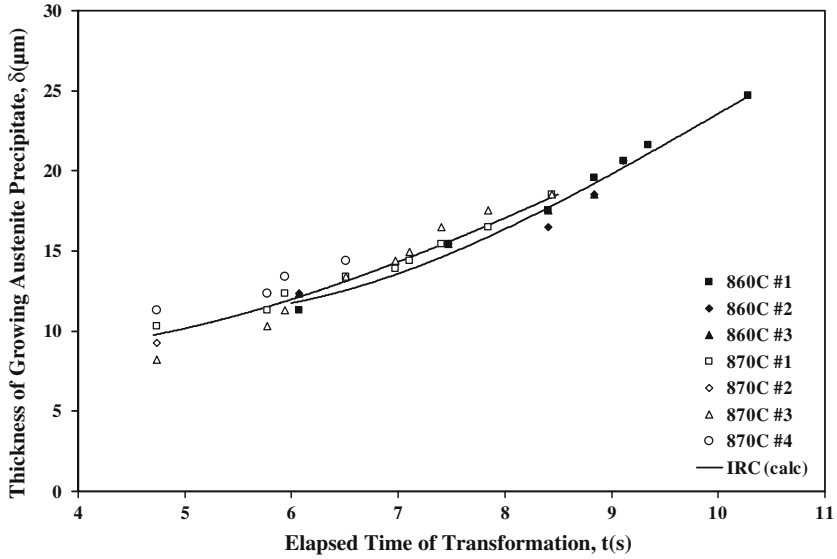

Fig. 9—Front migration data from CSLM for 870 °C and 860 °C "isothermal" experiments, at temperatures above T0, compared to the interface reaction control model for a moving austenite/ferrite boundary. Curves represent an interface reaction control model fit to the data.

boundaries in iron and iron alloys in comparing the present work to previous results (rather than activation enthalpies and pre-exponential factors). Mobility can been determined from the following type of relationship:

$$M = \frac{v \cdot V_m}{\Delta g \cdot N_A} \quad (\mathrm{m}^4 \cdot \mathrm{J}^{-1} \cdot \mathrm{s}^{-1}) \qquad [2]$$

where v is the velocity of the migrating interface, M is the mobility, Δg is the free energy change associated with the transformation (per atom), N_A is Avogadro's number, and V_m is the molar volume ($\sim 7 \times 10^{-6}$ m^3/mol for Fe). The results of these studies, along with the present results, are contained in Figure 10. More detailed information about the regions indicated in this figure are contained in Table IV, including alloy content, the transformation that was studied, the method used, and any interstitial impurities that were known to exist in the studied samples. Studies of three different kinds of migrating interfaces have been included: ferrite/ferrite during grain growth and recrystallization,[25,40,41] ferrite/austenite during heating,[7,18] and austenite/ferrite during cooling.[42,43,44] Despite the relatively large range of data that has been reported, the current results do appear to compare favorably to results that have been reported for Fe-1Mn alloys, and fall into the same general range as other dilute substitutional alloys.

D. *Metallographic Observations of Carbon Redistribution*

As a confirmation of the mechanism of transformation during nonisothermal growth, an analysis of the microstructure and carbon distribution before and after heat treating has also been investigated. The concentration of carbon in austenite has a strong influence on the decomposition products during quenching; austenite with more carbon dissolved in it would decompose into bainite, martensite, and/or pearlite (depending on the cooling rate). Thus, if the transformation occurred solely by the long-range diffusion of carbon, the austenite would have a relatively even distribution of carbon and the resulting microstructure would be unrelated to the prior microstructure. On the other hand, if there is an uneven distribution of carbon in the austenite before quenching—as would be the case if the ferrite regions transformed to austenite by a partitionless, interface-controlled mechanism—there should be a distinct difference between the resulting microstructure in what were ferrite and pearlite regions before heat treating. To test this hypothesis, experiments were carried out by marking samples in various locations so that the microstructure of a particular region could be examined before and after heat treating in the CSLM. The same regions were observed in the CSLM as well, to ensure that the samples were quenched (in Helium) immediately after the transformation was complete and therefore no homogenization could occur in the austenitized state. The distance that carbon would be able to travel behind a migrating interface must be considered in order for this assumption to be accurate. This distance can been approximated by $(Dt)^{0.5}$; for austenite at the ferrite eutectoid composition ($D = 6.3 \times 10^{-8}$ cm^2/s at 900 °C, according to Reference 46), which it would have immediately after a partitionless transformation from ferrite, a carbon diffusion distance of ~5 μm would occur during the < 5 seconds of transformation. This is a significant value, but still less than the 25 to 40 μm growth distance of the observed fronts. Before each experiment, a nital-etched sample was observed in the SEM, as shown in Figures 11(a) and 12(a). The SEM images elucidate ferrite regions as dark gray and pearlite regions as white. After the heat treatment, the samples were lightly repolished with a 0.05-μm alumina slurry to ensure minimal removal of material. This surface was also etched with nital, to expose the size and shape characteristics of the resulting austenite decomposition microstructure. In order to enhance the appearance of carbides in this microstructure, an alkaline sodium picrate (picric acid in a sodium hydroxide solution) stain was used to color carbon-rich areas with an orange or blue color. Images of the resulting structures were then observed with an optical microscope. This sequence of steps was carried out for samples transformed nonisothermally at 0.5 and 20 deg/s heating rates. The prior and resulting microstructures, as well as the evolving microstructures during the heat treatment, of the exact same regions of the surface for both heating rates have been presented in a series (Figures 11(a) through (f) and 12(a) through (f)) starting with (a) the SEM images, then (b) through (e) four CSLM stills, and finally (f) the optical micrographs. In these micrographs, the following features should be noted: (1) large ferrite and pearlite regions in the starting microstructures; (2) dark needlelike shapes in the evolving microstructure formed during decomposition;

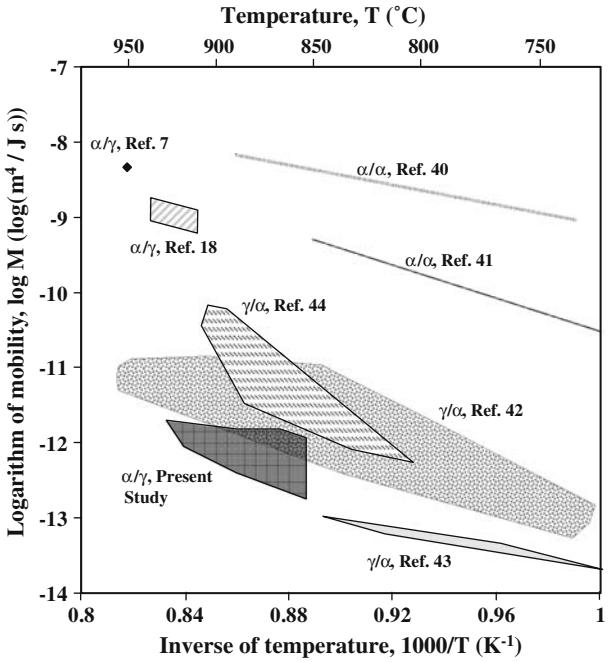

Fig. 10—Comparison of front mobilites for recrystallization of ferrite, ferrite to austenite, and austenite to ferrite in iron and substitutional iron alloys. Detailed information about each study is contained in Table IV.

Table IV. Selected Information about Mobility Data Contained in Figure 10; HTME Means That a Heat Treatment Followed by Metallographic Examination was Used as an Experimental Method; Mobilities are Given as Log ($m^4/J \cdot s$), and Impurities are in Mass Parts per Million

Reference	Material (Wt Pct)	Phase Change Studied	Method	Temperature Range (°C)	Experimental Mobility (Log M)	Known Interstitial Impurity (ppm)
7	zone-refined iron	$\alpha \rightarrow \gamma$	HTME	950	8.34	C(4)
40, 25	zone-refined iron	$\alpha \rightarrow \alpha$ (grain growth)	HTME	737 to 890	8.16 to 9.02	C(<10), N(<20)
41, 25	zone-refined iron	$\alpha \rightarrow \alpha$ (grain growth)	HTME	604 to 851	9.30 to 12.1	C + N (<30)
18	99.995 pct Fe	$\alpha \rightarrow \gamma$	CSLM	914 to 920	8.86 to 8.97	N(2), C(<1)
18	IF steel	$\alpha \rightarrow \gamma$	CSLM	914 to 932	8.76 to 9.18	C(50 ± 10), N(60)
44	Fe-1Co	$\gamma \rightarrow \alpha$	DTA	896 to 905	10.19 to 10.23	C(20), N(1)
44	Fe-2.1Co	$\gamma \rightarrow \alpha$	DTA	898 to 907	10.45 to 10.50	C(20), N(2)
44	Fe-0.9Cu	$\gamma \rightarrow \alpha$	DTA	844 to 883	11.48 to 11.70	C(20), N(10)
44	Fe-1.88Cu	$\gamma \rightarrow \alpha$	DTA	807 to 831	12.08 to 12.23	C(20), N(28)
42	Fe-1Co	$\gamma \rightarrow \alpha$	dilatometry	881 to 895	11.00 to 11.13	C(20), N(1)
42	Fe-2.1Co	$\gamma \rightarrow \alpha$	dilatometry	899 to 905	10.90 to 11.05	C(20), N(2)
42	Fe-0.9Cu	$\gamma \rightarrow \alpha$	dilatometry	854 to 858	11.22 to 11.47	C(20), N(10)
42	Fe-1.88Cu	$\gamma \rightarrow \alpha$	dilatometry	794 to 818	11.72 to 11.80	C(20), N(28)
42	Fe-0.8Mn	$\gamma \rightarrow \alpha$	dilatometry	847 to 849	11.02 to 11.33	C(30), N(7.5)
42	Fe-1.9Mn	$\gamma \rightarrow \alpha$	dilatometry	731 to 738	12.88 to 13.21	C(11), N(110)
42	Fe-0.5Al	$\gamma \rightarrow \alpha$	dilatometry	947 to 951	10.97 to 11.25	C(11), N(75)
42	Fe-1.8Cr	$\gamma \rightarrow \alpha$	dilatometry	830 to 836	11.91 to 12.32	C(11), N(103)
43	Fe-0.86Mn	$\gamma \rightarrow \alpha$	DTA	817 to 842	13.02 to 13.17	C(<45), N(<25)
43	Fe-1.94Mn	$\gamma \rightarrow \alpha$	DTA	727 to 767	13.39 to 13.68	C(<45), N(<25)

(3) black lines indicating boundaries between any combination of ferrite, bainite, or martensite features in the optical micrographs; and (4) orange and blue tinting, which indicate the presence of carbon. Because the needlelike structures observed to form in the CSLM correlate with high carbon (orange/blue) in the optical micrographs, it follows that these must be bainite or martensite laths/plates. This is further supported by the temperatures in which these structures have been observed to form, between 550 °C and 250 °C. Needle-like shapes that are not strongly colored suggest Widmanstätten ferrite laths. For the 0.5 K/s heating

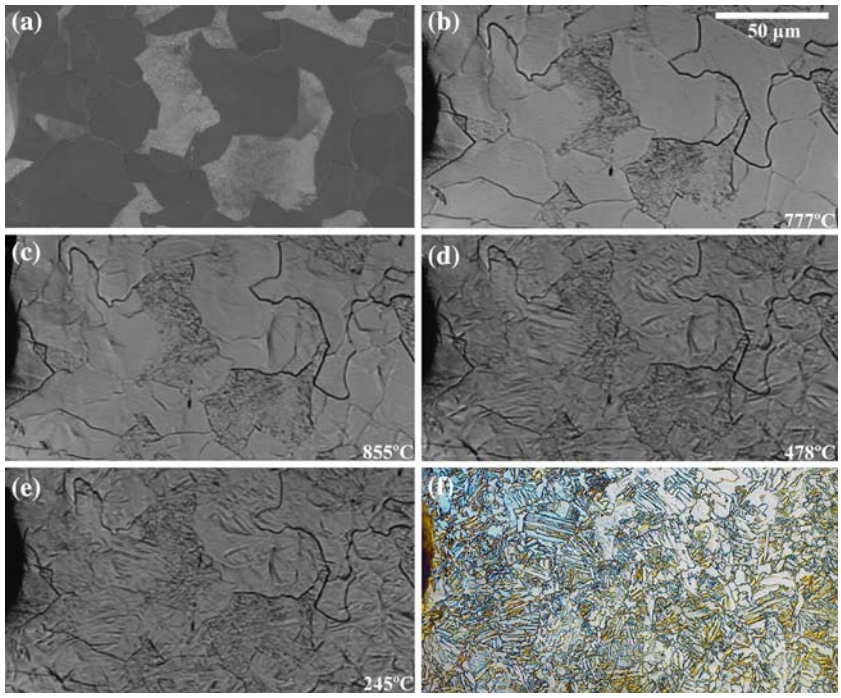

Fig. 11—(*a-f*): Series of micrographs for same location in a 4118 sample: (*a*) starting microstructure, etched with nital, as observed in the SEM; (*b-c*) austenitization of ferrite grains during 0.5 K/s heating, (*d*) completion of austenite to ferrite/bainite transformation, (*e*) completion of austenite to martensite transformation as observed in CSLM; (*f*) optical micrograph of resulting structure etched with nital to show structure and tinted orange and blue to indicate carbon rich areas. Sample was quenched in He gas immediately after the completion of austenitization.

rate, the microstructure after heat treating consists of small ferrite grains, lath ferrite, lath martensite, and bainite (carbon-rich needle-shaped regions). The size distribution of the ferrite grains and martensite laths is fairly uniform, and the carbon is evenly distributed with the exception of a few areas where larger ferrite grains exist. It is quite apparent that no correlation exists between the carbon poor areas of the heat-treated microstructure in Figure 11(f) and the location of the large ferrite grains seen in Figure 11(a) before the heat treatment. This means that the ferrite regions in the starting microstructure do not end up containing more or less carbon than the pearlite regions. Thus, all of the austenite must have transformed by a long-range diffusion-controlled mechanism that resulted in austenite that had a uniform distribution of carbon throughout before decomposition. For the 20 K/s heating rate (Figure 11), the same features in the heat-treated structure are present, but here, there are some regions where the ferrite grains are much larger, and regions where the lath martensite and bainite are much finer with a deeper blue/orange tint, than for the 0.5 K/s experiment (Figure 10(f)). The carbides are more concentrated in the martensite/bainite regions as well. The locations of the larger, carbon-poor ferrite grains—labeled (X, Y, Z)—in Figure 12(f) correlate well with the location of prior ferrite grains—also labeled (X, Y, Z)—in Figure 12(a), while the surrounding fine, carbon-rich martensite/bainite regions match the white prior pearlite colonies. Based on the ~5-μm diffusion distance of carbon behind a migrating interface previously mentioned, the smaller size of the carbon poor areas in Figure 12(f), compared to Figure 12(a), is expected. This also explains why smaller ferrite grains in Figure 12(a) do not correlate at all to Figure 12(f). Also, there is the appearance of more martensite between Figures 12(d) and (e), the small needlelike structures, as indicated by the arrows in Figure 12(e), that form at the lowest temperatures (between 250 °C and 400 °C, a typical martensite growth range)—in the regions that were initially pearlite. These structures appear within one frame (less than 1/30th of a second), which also supports the assumption that they are martensite. This is especially noticeable in what was the large pearlite region in the left of the micrographs near the fiducial mark. This is consistent with the fact that there must have been more carbon in these regions than in those regions that were initially ferrite grains once the entire sample had been austenitized. Thus, at the 20 K/s heating rate, it is apparent that the austenite that decomposed did not have a uniform distribution of carbon; austenite in prior ferrite grains formed by a partitionless mechanism and remained at a very low carbon concentration, while surrounding austenite in prior pearlite colonies maintained a near-eutectoid composition. These micrographs further support the hypothesis that a partitionless, interface-controlled transformation occurs during sufficiently rapid heating at temperatures above T_0. One possible implication of this result is that a dual-phase (ferrite + martensite) microstructure could be achieved through a very rapid heat treating procedure incorporating a rapid heating followed by a rapid quench, and would not require an extended intercritical annealing step. Grain refinement would occur by the process as well, as each initial

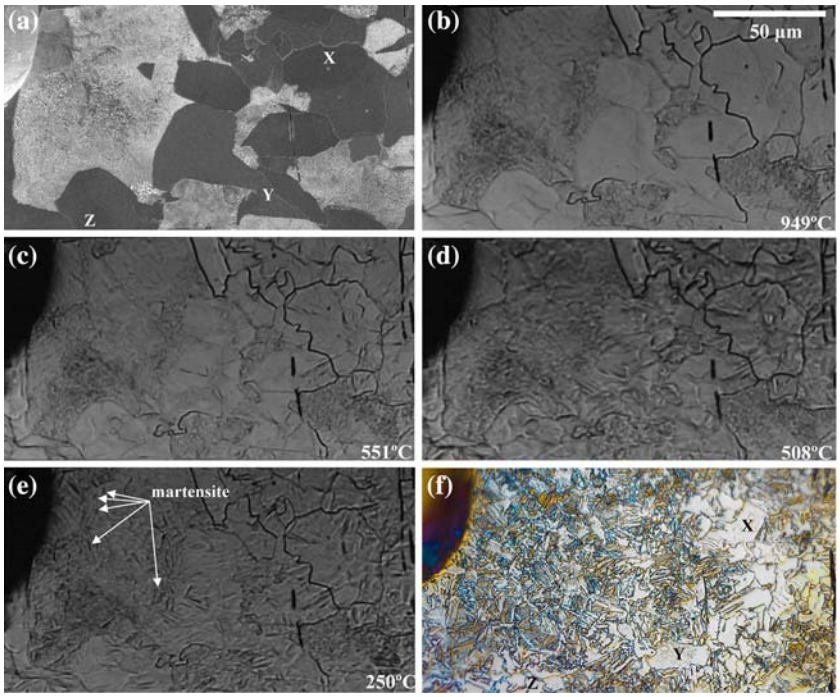

Fig. 12—(*a-f*): Series of micrographs for same location in a 4118 sample: (*a*) starting microstructure, etched with nital, as observed in the SEM; (*b*) completion of austenitization of ferrite grains during 20 K/s heating, (*c-d*) austenite to ferrite/bainite transformation, (*e*) completion of austenite to martensite transformation as observed in CSLM; (*f*) optical micrograph of resulting structure etched with nital to show structure and tinted orange and blue to indicate carbon rich areas. Sample was quenched in He gas immediately after the completion of austenitization.

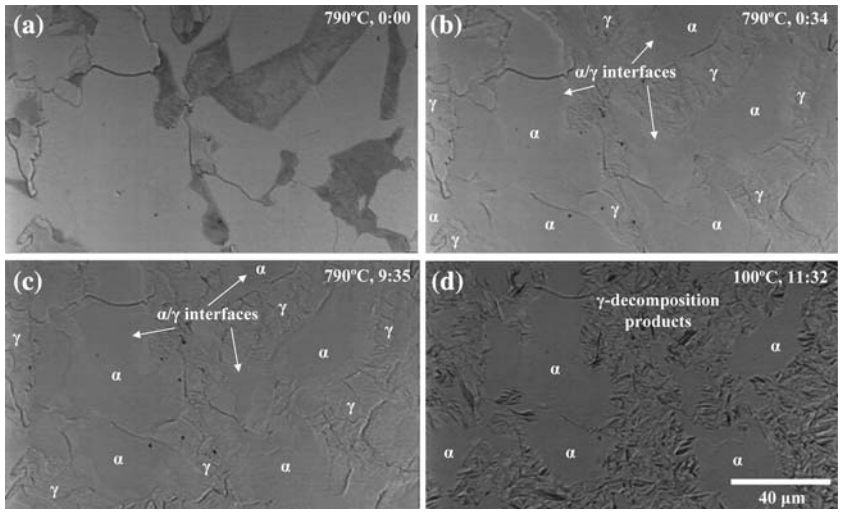

Fig. 13—(*a-d*): CSLM still images show (*a*) initial structure, (*b-c*) austenite front migration during isothermal 790 °C transformation, and (*d*) the resulting austenite decomposition microstructure in the transformed regions during a quench in helium gas, with the untransformed ferrite remaining unchanged throughout the quench. This supports the hypothesis that the fronts visible in (*b-c*) are austenite/ferrite interfaces.

ferrite grain would result in several smaller ferrite grains, while the initial eutectoid regions would result in a very fine martensite/bainite structure.

E. *CSLM: Isothermal Front Migration*

If there is a transition from long-range diffusion control to interface reaction control, a set of isothermal experiments that spanned a suitable temperature range should support this hypothesis by resulting in distinct differences in the time dependence of interface migration rates above and below T_0. In Section D, it has already been demonstrated that the attempted isothermal experiments at 860 °C and 870 °C, despite the nonuniform temperature, behave in a manner consistent with the interface reaction control model. Although the temperature is not constant here, the interface reaction-controlled model curves in Figure 9 are very close to linear, with a slight upward curvature, even while the heating rate is slowing rapidly during the transformation. During nonisothermal experiments in Section D, at temperatures below T_0, there was an approximately linear slope at constant heating rates, and one would expect that if the heating rate was slowing during this regime, that slope would deviate negatively from linear, not the other way around. It seems reasonable then that if the desired temperature above T_0 could be reached very quickly and held constant at these temperatures, there would be no upward curvature—the slopes would be linear and therefore consistent with interface reaction control.

Figures 13(a) through (d) are a series of CSLM stills showing isothermal austenite formation at 790 °C, followed by a subsequent quench in He gas. It is quite apparent from (d) that the fronts observed in (b) and (c) are the boundaries between austenite and ferrite, as the decomposition products that appear during the quench do not appear in the untransformed ferrite regions. Figure 14(a) shows an example of a set of isothermal front migration curves at a temperature below T_0, also at 790 °C, as observed in the CSLM. There is significant decay of the migration rate with time. As indicated in Figure 14(b), an excellent fit of precipitate thickness to $t^{1/2}$ in an initial growth period is observed; deviation from the model at later times will be discussed subsequently. The calculated slopes for the initial parabolic regime, determined in the same way for all of the isothermal experiments, have been listed in Table V. Sekerka and Wang[45] have presented a solution to the semi-infinite moving boundary diffusion-controlled growth situation consistent with the observations of the present study. The boundary position can be related to time by the following relationship:

$$\xi = K\sqrt{4D^{\gamma}t} \qquad [3]$$

where ξ is the interface position (equivalent to the austenite precipitate thickness, δ, in the present investigation); D is the rate-controlling diffusion coefficient, in this case, that of the austenite; t is the time of transformation; and K is a dimensionless constant determined by solving

$$K = -\frac{1}{\sqrt{\pi}}\sqrt{D^{\alpha}/D^{\gamma}}Q^{\alpha}S^{\alpha}\frac{\exp\left(-K^2D^{\gamma}/D^{\alpha}\right)}{1-\operatorname{erf}\left(K\sqrt{D^{\gamma}/D^{\alpha}}\right)} + \frac{1}{\sqrt{\pi}}Q^{\gamma}S^{\gamma}\frac{\exp\left(-K^2\right)}{1+\operatorname{erf}(K)} \qquad [4]$$

The carbon diffusion coefficient in austenite used in Eqs. [2] and [3] was calculated according to Ågren[46] and in ferrite according to Reference 47. The S^{α} and S^{γ} are supersaturations, given by

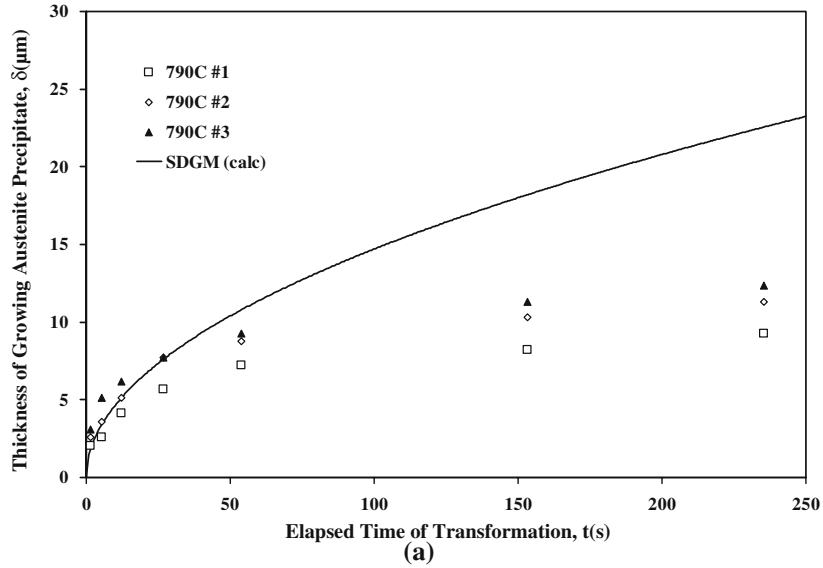

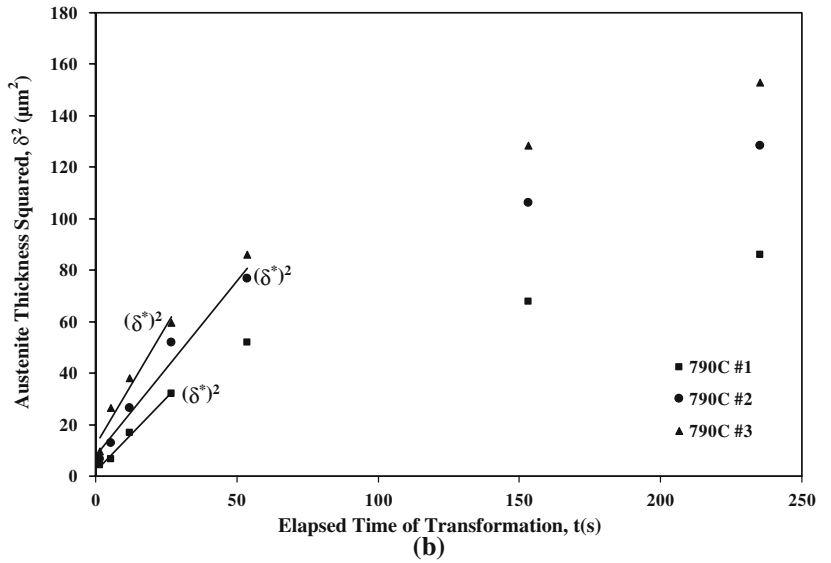

Fig. 14—(*a*): Front migration data from a 790 °C isothermal CSLM experiment, compared to the diffusion model for a moving austenite/ferrite boundary in semi-infinite medium. Other isothermal results are similar in appearance. (*b*): Front position squared vs. time data from a 790 °C isothermal CSLM experiment; the slope is used to determine the experimentally measured K (diffusion-controlled growth model constant), and indicates the critical thickness, δ^*, at which boundary migration rate deviates from the semi-infinite extent diffusion model.

$$S^{\alpha} = \frac{\left(C^{\alpha}_{\text{interface}} - C^{\alpha}_{\infty}\right)}{\left(C^{\gamma}_{\text{interface}} - C^{\alpha}_{\text{interface}}\right)}$$

and

$$S^{\gamma} = \frac{\left(C^{\gamma}_{\infty} - C^{\gamma}_{\text{interface}}\right)}{\left(C^{\gamma}_{\text{interface}} - C^{\alpha}_{\text{interface}}\right)} \qquad [6]$$

The interface concentrations are determined from the paraequilibrium lines in the phase diagram in Figure 6, and the semi-infinite initial carbon concentrations are assumed to be near the eutectoid compositions. It has already been established that this is a reasonable approximation for the ferrite, as the paraequilibrium composition of carbon in the proeutectoid ferrite is very close to the equilibrium composition. The initial carbon concentration of the austenite that formed from the pearlite regions is more uncertain; it will be assumed,

Table V. Slopes, in (μm^2/s), of Initial Parabolic Regime during Isothermal Austenite Front Migration

Experiment	Front 1	Front 2	Front 3	Front 4
790 °C	1.12	1.35	1.83	—
800 °C	0.39	0.41	1.67	—
810 °C	3.12	4.05	4.78	—
820 °C	5.08	—	—	—
830 °C	15.00	13.53	7.97	—
840 °C	33.73	32.75	32.45	16.00
850 °C	21.48	9.41	31.62	11.68

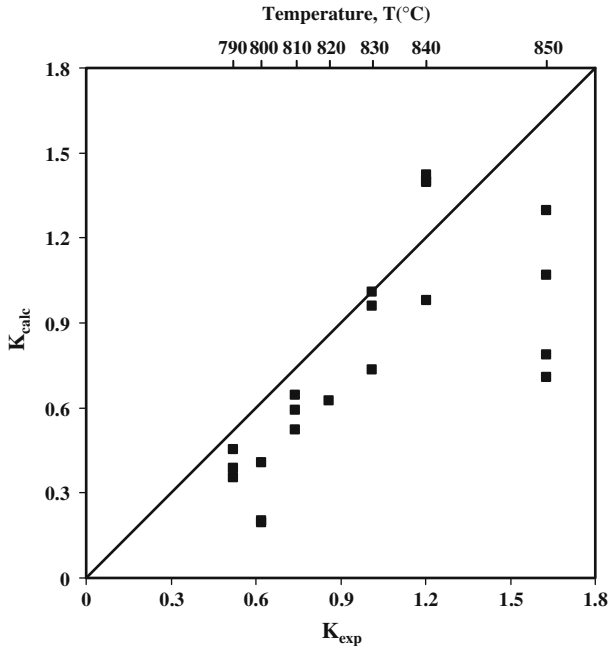

Fig. 15—Comparison of the experimentally determined semi-infinite extent diffusion model boundary migration constant (K_{exp}), with calculated values (K_{calc}) at the isothermal temperatures indicated.

however, that the deviation will not be so great as to disrupt the general trend of these calculations. The Q's in Eq. [3] refer to volume changes associated with the phase change and have been disregarded in this analysis. The calculated lines, according to Eqs. [2] through [5], are shown in Figure 14(a) and designated "SDGM" (semi-infinite diffusion-controlled growth model). Figure 15 shows the relationship between the calculated K using the preceding method and the experimentally measured K, using the slopes in Table IV and Eq. [2]. There is good agreement between the two values for most of the fronts, with the exception of a few outliers, especially at 850 °C. One possible explanation for the outliers at this temperature is that, because a significant portion of the transformation occurs before the temperature is isothermal and stable, these fronts have already entered the stage of the transformation where the diffusion fields are no longer semi-infinite in nature and thus have already deviated from the initial semi-infinite solution growth regime. The general trend is for the model to underpredict the value of K. This is most likely the result of the uncertainty in the carbon concentration in the austenite, which had initially formed from the eutectoid regions of the starting microstructure. An increase in this concentration would result in a larger S^{γ} and a larger K, and would more closely match the experimental data. How much deviation there is cannot be directly known (the austenite cannot be preserved for compositional analysis), but overall the mechanisms in both regimes would remain consistent.

A simplified model, using an approach similar to Zener[48] for the diffusion-controlled growth of austenite in prior ferrite regions, has been proposed by Caballero *et al.*,[13] which suggests that two stages of diffusion control do exist. The model considers that growth will occur with a boundary layer in the growing austenite and a constant composition of carbon in the ferrite. During the first stage, the edge of the diffusion field has not yet depleted the center of the prior eutectoid colony (now austenite) of carbon, and the composition at the end of the boundary layer remains constant at the eutectoid composition and could be considered as a semi-infinite configuration. At later times, the diffusion field will begin to impinge upon that of an austenite front that is growing from the same eutectoid colony, or with an edge of the prior eutectoid colony, and the carbon concentration at the edge of the boundary layer must start to decrease. When this happens, the migration rate will be expected to decrease at a more rapid, nonparabolic rate.[45] An analysis of the effect of microstructure size features was carried out to verify this mechanism. In the course of determining the cutoff where the initial parabolic regime is satisfied, as in Figure 14(b), the critical austenite precipitate thickness, δ^*, can be compared to the adjacent prior eutectoid colony size (measured perpendicular to the front migration direction) from which that front grows. These two values should be closely related, as a larger eutectoid austenite region would mean that the semi-infinite solution should be valid over a longer distance before overlap with another diffusion field will occur. As an initial estimate, it is suggested that this critical thickness will occur when it is equal to the half-thickness of the adjacent prior eutectoid colony. A plot relating these values is provided in Figure 16. The thickness at which the semi-infinite diffusion model breaks down, relative to the adjacent pearlite thickness, seems to increase with temperature. There is significant scatter in the data, even

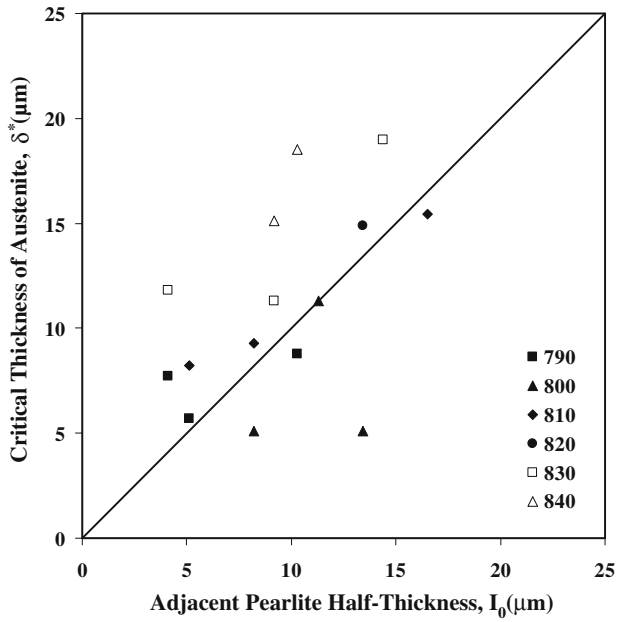

Fig. 16—Comparison of the prior adjacent pearlite size to the distance at which austenite fronts deviate from the semi-infinite extent diffusion-controlled growth model.

at a single temperature; this may be due to the three-dimensional nature of the eutectoid colonies, which makes it difficult to determine the actual size of the eutectoid colonies based on their appearance in the plane of the surface. Some of the points that deviate significantly could therefore result from a much larger or smaller eutectoid colony below the plane than that which is observed. This indicates that a more comprehensive finite diffusion model that incorporated the initial size of the austenite precipitates upon dissolution of the eutectoid regions might not be useful in this case. Thus, future work with such a diffusion model would require a microstructure with fewer or smaller eutectoid colonies, or perhaps with large spheroidized carbide particles, as in Reference 10. Nonetheless, Figure 16 does show some agreement and at least supports the possibility that a model sensitive to the size features of the initial microstructure would be useful.

IV. SUMMARY AND CONCLUSIONS

The kinetics of austenitization in mixed ferrite/eutectoid steel have been studied through the use of confocal scanning laser microscopy, dilatometry, and electron microscopy. The following conclusions can be drawn from the combination of results of these experimental methods.

1. Austenite front migration in the ferrite regions of a mixed microstructure, ferrite/eutectoid steel appears to be controlled by long-range diffusion of carbon at temperatures below T_0, and by an interface reaction, proceeding through a massivelike mechanism, at temperatures above. This has been confirmed in both nonisothermal and isothermal experiments.
2. Nonisothermal experiments are consistent with an interface reaction control model developed for pure iron in the expected temperature range. The interface mobility reported compares favorably to previous studies of austenite-to-ferrite transformation in dilute, substitutionally alloyed iron.
3. For temperatures below T_0 and prior to expected diffusion field impingements, the diffusion-controlled rate constants corresponding to measured front migration under isothermal conditions compare quite favorably to those calculated by a semi-infinite, moving boundary diffusion model.
4. The diffusion-controlled growth during isothermal heat treating conditions below T_0 occurs in two distinct stages; this corresponds to the time before and after the carbon diffusion fields in the austenite that had formed in the prior eutectoid regions impinge with each other or with the edge(s) of the austenite grain, as has been suggested by previous investigations.
5. Carbon distribution in a sample that appears to have transformed partially by long-range diffusion of carbon and partially by a massive transformation is consistent with such a mixed mechanism. When subjected to a fast heating rate, the carbon-rich and carbon-poor regions remain roughly in the same locations, resulting in a unique microstructure. This correlation is not observed for a slow heating rate where the transformation occurs entirely in the diffusion-controlled regime.

ACKNOWLEDGMENTS

This project was performed through financial support from the National Science Foundation under CAREER Grant No. DMR 0348818. The authors thank the Timken Steel Corporation for materials used in the investigation.

REFERENCES

1. W.T. Reynolds, Jr., M. Enomoto, and H.I. Aaronson: *Proc. Int. Conf. on Phase Transformation in Ferrous Alloys*, Philadelphia, PA, Oct. 4–6, 1983, A.R. Marder and J.I. Goldstein, eds., AIME, Warrendale, PA, pp. 155–200.
2. J.M. Rigsbee and H.I. Aaronson: *Acta Mater.*, 1979, vol. 27, pp. 351–63.
3. J.M. Rigsbee and H.I. Aaronson: *Acta Mater.*, 1979, vol. 27, pp. 365–76.
4. C.A. Dube, H.I. Aaronson, and R.F. Mehl: *Rev. Met.*, 1958, vol. 55, p. 201.
5. G. Spanos and M.G. Hall: *Metall. Mater. Trans. A*, 1996, vol. 27A, pp. 1519–34.
6. K.R. Kinsman, E. Eichen, and H.I. Aaronson: *Metall. Trans. A*, 1975, vol. 6A, pp. 303–17.
7. G.R. Speich and A. Szirmae: *Trans. TMS-AIME*, 1969, vol. 245, pp. 1063–74.
8. A. Roosz, Z. Gaesi, and E.G. Fuchs: *Acta Mater.*, 1983, vol. 31(4), pp. 509–17.
9. G.R. Speich, V.A. Demarest, and R.L. Miller: *Metall. Trans. A*, 1981, vol. 12A, pp. 1419–28.
10. R.R. Judd and H.W. Paxton: *Trans. TMS-AIME*, 1968, vol. 242, pp. 206–15.
11. F.G. Caballero, C. Capdevila, and C. de Garcia Andres: *Iron Steel Inst. Jpn. Int.*, 2001, vol. 41, pp. 1093–1102.
12. G. Molinder: *Acta Mater.*, 1956, vol. 4, pp. 565–71.
13. F.G. Caballero, D. San Martin, C. Capdevila, A. Garcia-Junceda, and C. Garcia de Andres: *Proc. Int. Conf. on Solid-Solid Phase Transformations in Inorganic Materials 2005*, Phoenix, AZ, May 29–June 3, 2005, James M. Howe, David E. Laughlin, Jong K. Lee, Ulrich Dahmen, and William A. Soffa, eds., TMS, Warrendale, PA, 2005, vol. 1, pp. 707–12.
14. F.G. Caballero, C. Capdevila, and C. de Garcia Andres: *Metall. Mater. Trans. A*, 2001, vol. 32A, pp. 1283–91.
15. F.G. Caballero, C. Capdevila, D. San Martin, and C. Garcia de Andres: *Proc. Symp. on the Thermodynamics, Kinetics, Characterization, and Modeling of Austenite Formation and Decomposition*, MS&T Meeting, Chicago, IL, E.B. Damm and M.J. Merwin, eds., TMS, Warrendale, PA, pp. 457–74.
16. M. Hunkel, H. Surm, Th. Lübben, O. Kessler, F. Hoffman, and P. Mayr: *Proc. Symp. on the Thermodynamics, Kinetics, Characterization, and Modeling of Austenite Formation and Decomposition*, MS&T Meeting, Chicago, IL, E.B. Damm and M.J. Merwin, eds., TMS, Warrendale PA, pp. 475–89.
17. E. Schmidt, Y. Wang, and S. Sridhar: *Metall. Mater. Trans. A*, 2006, vol. 37A, pp. 1799–1809.
18. E. Schmidt, A. Bednar, S. Roberts, D. Soltesz, and S. Sridhar: *J. Iron Steel Inst. Jpn.*, 2006, vol. 46, pp. 1500–1509.
19. E. Schmidt and S. Sridhar: *Proc. Int. Conf. on Solid-Solid Phase Transformations in Inorganic Materials 2005*, Phoenix, AZ, May 29–June 3, 2005, James M. Howe, David E. Laughlin, Jong K. Lee, Ulrich Dahmen, and William A. Soffa, eds., TMS, Warrendale, PA, 2005, vol. 2, pp. 551–68.
20. E. Schmidt, E.B. Damm, and S. Sridhar: *Proc. Int. Conf. on New Developments in Long and Forged Products: Metallurgy and Applications*, AIST, Warrendale, PA, 2006, pp. 203–17.

21. D. Phelan: Ph.D. Thesis, University of Wollongong, Wollongong, Australia, 2002.
22. R.J. Dippenaar and D.J. Phelan: *Metall. Mater. Trans. B*, 2003, vol. 34B, pp. 495–501.
23. H. Yin, T. Emi, and H. Shibata: *Acta Mater.*, 1999, vol. 47, pp. 1523–35.
24. M.G. Mecozzi, J. Sietsma, S. Van Der Zwaag, M. Apel, P. Schaffnit, and I. Steinbach: *Proc. Symp. on the Thermodynamics, Kinetics, Characterization and Modeling of Austenite Formation and Decomposition*, MS&T Meeting, Chicago, IL, 2003, E.B. Damm and M.J. Merwin, eds., TMS, Warrendale, PA, 2003, pp. 353–66.
25. M. Hillert: *Metall. Trans. A*, 1975, vol. 6A, pp. 5–19.
26. M. Hillert: *Metall. Mater. Trans. A*, 2002, vol. 33A, pp. 2299–2308.
27. D.A. Porter and K.E. Easterling: *Phase Transformations in Metals and Alloys* 2ne ed., Stanley Thornes Publishers Ltd, United Kingdom, 2000, 143–48.
28. H.M. Clark and C.M. Wayman: *Phase Transformations*. ASM, Metals Park, OH, pp. 59–114.
29. J.D. Watson and P.G. McDougall: *Acta Metall.*, 1973, vol. 21, pp. 961–73.
30. W.W. Mullins: *J. Appl. Phys.*, 1959, vol. 30(1), pp. 77–83.
31. A.W. Bowen and G.M. Leak: *Metall. Trans.*, 1970, vol. 1, p. 2767.
32. K. Nohara and K. Hirano: *J. Jpn. Inst. Met.*, 1973, vol. 37, p. 51.
33. A.P. Sutton and R.W. Balluffi: *Interfaces in Crystalline Materials* Oxford University Press IncNew York, NY, 1995, 522–97.
34. T.B. Massalski: *Phase Transformations*, Seminar of the American Society of Metals, ASM, Metals Park, OH, 1970 pp. 433–86.
35. T.B. Massalski, W.A. Soffa, and D.E. Laughlin: *Metall. Mater. Trans. A*, 2006, vol. 37A, pp. 825–31.
36. P. Shewmon: *Diffusion in Solids* McGraw-Hill Book CoNew York, NY, 1963,.
37. A.M. Brown and M.F. Ashby: *Acta Metall.*, 1980, vol. 28, pp. 1085–1101.
38. V. Paidar and P. Lejcek: *Mater. Sci. Forum*, 2005, vol. 482, pp. 63–70.
39. M. L. Hillert and L. Höglund: *Scripta Mater.*, 2006, vol. 54, pp. 1259–63.
40. V.I. Ivanov and K.A. Osipov: *Sov. Phys. Dokl.*, 1961, vol. 6, pp. 425–28.
41. Hsun Hu: *Can. Metall. Q.*, 1974, vol. 13(1), pp. 275–86.
42. J.J. Wits, T.A. Kop, Y. van Leeuwen, J. Seitsma, and S. van der Zwaag: *Mater. Sci. Eng. A*, 2000, vol. 283, p. 234.
43. G.P. Krielaart and S. van der Zwaag: *Mater. Sci. Technol.*, 1998, vol. 14, p. 10.
44. S.I. Vooijs, Y. Van Leeuween, J. Seitsma, and S. van der Zwaag: *Metall. Mater. Trans. A*, 2000, vol. 31A, pp. 379–85.
45. R.F. Sekerka and S.L. Wang: *Lectures on the Theory of Phase Transformations*, 2nd ed., H.I. Aaronson, ed., TMS, Warrendale, PA, (1999) pp. 231–83.
46. J. Ågren: *Scripta Metall.*, 1986, vol. 20, pp. 1507–10.
47. J.R.G. da Silva and R.B. McLellan: *Mater. Sci. Eng.*, 1976, vol. 26(1), pp. 83–87.
48. C. Zener: *J. Appl. Phys.*, 1949, vol. 20, pp. 950–53.